

## 변전위법 중합 과정에서 Polyaniline 핵 형성 및 성장 프로세스와 모폴로지 진화

김은옥<sup>†</sup> · 오현주 · 이언주 · 구형욱

수원대학교 공과대학 융합화학과

(2020년 2월 14일 접수, 2020년 3월 15일 수정, 2020년 3월 16일 채택)

### Nucleation-Growth Processes and Morphological Evolution of Polyaniline during Potentiodynamic Polymerization

Eunok Kim<sup>†</sup>, Hyunju Oh, Eonju Lee, and Hyungwook Koo

Department of Chemistry, The University of Suwon, Hwaseoung-si, Gyeonggi-do 18323, Korea

(Received February 14, 2020; Revised March 15, 2020; Accepted March 16, 2020)

**초록:** 변전위법 중합 과정에서 폴리아닐린의 핵 형성 프로세스 및 성장 프로세스를 모폴로지 진화와 연관하여 확인하였다. 필름증착은 초기에 2차원 성장 프로세스를 통한 점진적 핵 형성이 이루어지고, 이어서 3차원 성장 프로세스를 통한 점진적 핵 형성이 지배적이었다. 초기에는, ITO 전극 상에 부드럽고 치밀한 폴리아닐린 필름이 증착되었지만, 초기 단계 후에는 섬유상의 3차원 다공성 네트워크 구조가 관찰되었다. 순환 전압전류의 사이클이 증가함에 따라, 필름은 큰 자유 부피를 가지며 더욱 거칠고 다공성인 3차원 네트워크 구조가 되면서 도핑 레벨이 증가되었다. 결국, 증가된 도핑 레벨과 전하 캐리어 이동성의 향상으로 인해 폴리아닐린 필름의 면저항이 낮아졌다.

**Abstract:** The nucleation and growth processes associated with the morphological evolution of polyaniline during potentiodynamic polymerization have been investigated. Film deposition was first ruled by progressive nucleation with a two-dimensional growth process, and followed by progressive nucleation with a three-dimensional growth process. Initially, a smooth and compact polyaniline film was deposited on the indium tin oxide electrode, whereas a fibrous three-dimensional porous network structure was observed after the initial stage. As the number of cycles increased, the film became rougher and more porous three-dimensional network structure with higher free volume, resulting in higher doping levels. Finally, the increased doping levels and a higher charge carrier mobility lowered the sheet resistance of the polyaniline film.

**Keywords:** polyaniline, potentiodynamic, nucleation process, growth process, morphology.

## Introduction

Conducting polymers are polymers with conjugated  $\pi$ -electrons in a backbone, where the backbone can be transformed into an electrically conductive structure through a doping process. Among conducting polymers, polyaniline (PAni) has been widely studied because of its unique redox chemistry, adjustable electrochemical performance, and environmental and thermal stability. Moreover, potential applications such as electrochromic devices, rechargeable batteries, electromagnetic interference shielding, and sensors have led to extensive

research on PAni.<sup>1-4</sup> PAni can exist in different forms depending on its degree of oxidation: pernigraniline (fully oxidized with quinoid imine structures), leucoemeraldine (fully reduced with benzenoid amine structures), and emeraldine (half-oxidized with an equal number of imine and amine structures).<sup>5</sup>

The doping and de-doping of conducting polymers are reversible processes that occur almost no degradation of the polymer backbone. The non-redox doping of conducting polymers is a process in which the number of electrons associated with the polymer chain is kept constant, resulting in the rearrangement of energy levels.<sup>6</sup> The non-redox doping process in PAni involves the conversion of non-conducting base form of PAni (PAni-EB) into conducting emeraldine salt form of PAni (PAni-ES) after treatment with a protonic acid.<sup>7</sup> PAni-ES can be obtained through either chemical or electrochemical polym-

<sup>†</sup>To whom correspondence should be addressed.  
eokim@suwon.ac.kr, ORCID<sup>®</sup>0000-0003-0344-0872  
©2020 The Polymer Society of Korea. All rights reserved.

erization. One of the significant advantages of the electrochemical method is the ability to deposit a conductive polymer film directly onto electrode surfaces in a simple and cost effective way, which ensures good ohmic contact between the electrode and the polymer.<sup>8</sup> Furthermore, the electrochemical method can be used to fine tune the thickness and morphology of the resulting film by controlling the total charge passed during deposition.<sup>3</sup>

The three electrochemical deposition methods for PANi are potentiostatic (constant potential), potentiodynamic (potential scanning or cyclic voltammetry), and galvanostatic (constant current). We compared the effects of the deposition method on the morphology and electrochemical properties of PANi, e.g., potentiodynamic *vs.* potentiostatic methods, and potentiodynamic *vs.* galvanostatic methods.<sup>8,9</sup> Upon these previous studies, we proposed a nucleation and growth processes by observing the morphological evolution of PANi during the potentiostatic and galvanostatic polymerization, respectively.<sup>7,9,10</sup> The nucleation and growth processes provided information at molecular level of how the polymeric film is generated on the electrode surface, thus enabling the development of polymerization strategies to obtain polymer coatings with desired properties.<sup>11</sup> The potentiodynamic polymerization of aniline involves scanning the potential of the working electrode linearly and repeatedly, from initial to final values in forward and reverse directions until the desired amount of polymer has been deposited.

In this work, the resulting PANi films were characterized by scanning electron microscopy (SEM), Fourier-transformed infrared (FTIR) spectroscopy, Ultraviolet-Visible (UV-Vis) spectroscopy, and sheet resistance measurements to get information about the chemical structure, doping level, morphology and changes in electrical conductive properties as a function of the number of cyclic voltammetry (CV) cycles. Finally, in order to understand the nucleation and growth processes of the PANi, their morphological evolution was further observed during the potentiodynamic polymerization, and the effect of polymer morphology on the electrical conductive properties of PANi films was investigated.

## Experimental

**Materials.** Aniline ( $\geq 99.0\%$ , Duksan Pure Chemicals) was purified by double distillation before use. Hydrochloric acid (HCl, 37.0%, Duksan Pure Chemicals) and dimethyl sulfoxide (DMSO,  $\geq 99.0\%$ , Sigma-Aldrich) were used as received.

**Potentiodynamic Polymerization.** The PANi films were obtained by cyclic voltammetry for seven different cycles: 1, 3, 5, 10, 20, 30 and 40, which are denoted for simplicity as PANi-1cy, PANi-3cy, PANi-5cy, PANi-10cy, PANi-20cy, PANi-30cy and PANi-40cy, respectively. A three electrode system composed of an ITO working electrode, Ag/AgCl (3 M NaCl) reference electrode, and platinum plate counter electrode were used. The PANi film deposited at a scan rate of 10 mV/s and 40 successive cycles of potential between 0.0 and +1.1 V, using a battery cyler (WON A TECH, WBCS-3000). The experimental temperature was set at 273 K.<sup>8,12,13</sup>

**Characterization.** FTIR spectra were recorded on an FTIR/ATR 4100 Spectrometer (Jasco) in the attenuated total reflection (ATR) mode for wavenumbers of 600-2000  $\text{cm}^{-1}$ . UV-Vis spectra were recorded on an S-3100 Spectrophotometer (Scinco) for the wavelengths of 250-1100 nm. High-resolution scanning electron microscopy (SEM) imaging was performed using a LYRA 3 (Tescan) system. The thickness of the films was measured using a micrometer caliper. The four-point probe 2401 Source Measurement Unit (Keithley) was used to measure the sheet resistance of the films. In the case of the 1, 3 and 5 cycles, the thickness of the film was not thick enough for the measurement, so FTIR spectroscopy, UV-Vis spectroscopy, and sheet resistance measurements could not be performed.

## Results and Discussion

The nucleation and growth processes of conducting polymers involve several stages, beginning with the oxidation of the monomer at the anode followed by oligomerization and polymerization.<sup>1,14</sup> Figure 1 shows the cyclic voltammetric behavior for the polymerization of aniline during the first five successive cycles.

As shown in the first cycle (inset of Figure 1), a significant increase in anodic currents starts at about +0.90 V and corresponds to the oxidation of aniline, which is considered to be the rate-determining step.<sup>5</sup> The trace crossing, which appears as an anodic current observed on the reverse sweep of the first cycle, could result from slow follow-up reactions occurring at the diffusion layer in the vicinity of the electrode surface.<sup>3</sup> The oxidation of aniline results in the formation of PANi nuclei on the ITO surface, leading to the formation of oligomers that subsequently turn into the polymer after successive potential cycles.<sup>15</sup> The cyclic voltammogram shows that the current increases in each successive cycle, confirming the deposition

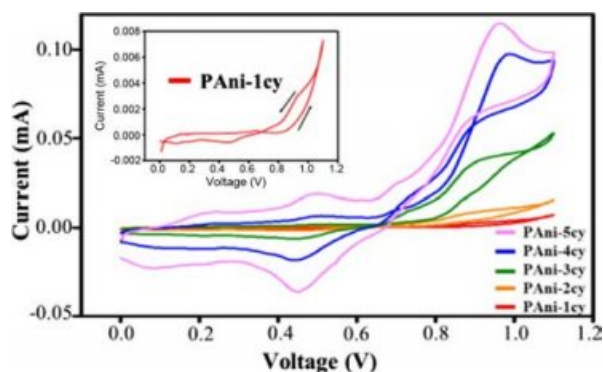


**Figure 1.** Cyclic voltammetric behavior of aniline polymerization for the first five successive cycles (Inset: first cycle).

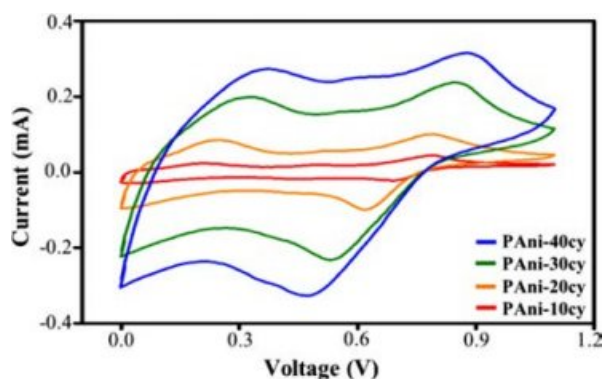


**Figure 2.** Cyclic voltammetric behavior recorded at different cycles (10, 20, 30, and 40) during the polymerization of aniline.

of PANi. As the potential of the working electrode changes with successive potential cycles, the deposited PANi changes between its non-conducting (de-doped) and conducting (doped) forms. Figure 2 shows the cyclic voltammetric behavior recorded at different cycles (10, 20, 30, and 40) during the polymerization of aniline. An increase in current is observed for each consecutive cycle, which indicates a steady growth in the thickness of the polymer film. Therefore, the thickness of the PANi film can be controlled by changing the number of cycles. Typical PANi CV curves exhibit two pairs of redox peaks, which are accompanied by charge transfer and mass transport. The first pair of redox peaks at the lower positive potential corresponds to the leucoemeraldine/polaronic emeraldine transition. The second pair of redox peaks at the higher potential corresponds to the polaronic emeraldine/permigraniline transition.<sup>9</sup> The anodic and cathodic currents increase rapidly with increasing cycle number because PANi has good catalytic activity to aniline. Such activity, in turn, promotes polymer deposition on the surface of the electrode and is there-

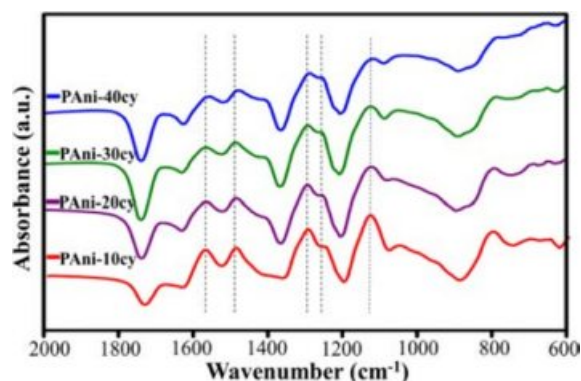


**Figure 3.** FTIR spectra of PANi obtained for different cycle numbers (10, 20, 30, and 40).

fore regarded as an autocatalytic process.<sup>16</sup> This result further shows that as the PANi layers grow on the ITO electrode with increasing the number of cycles, in which the actual electrode surface area gradually increases. The anodic peaks shift towards the positive direction, and the cathodic peaks shift towards the negative direction while simultaneously increasing the current. This shifting in peak potentials is consistent with the ohmic contribution to the overpotential.<sup>17</sup> Ohmic overpotential in an electrochemical cell is associated with both the ionic and electronic resistance, as well as contact resistance between all components.

FTIR spectroscopy in ATR mode is a powerful technique for analyzing the chemical structure of PANi film, and in particular, the oxidation state of its chains. Figure 3 shows the FTIR spectra of PANi obtained for different cycle numbers (10, 20, 30, and 40). Some low intensity peaks at  $\sim 620$ ,  $\sim 680$ , and  $\sim 790$   $\text{cm}^{-1}$  are ascribed to C-H bond vibrations in the benzenoid rings.<sup>18</sup> The characteristic band at  $\sim 1565$   $\text{cm}^{-1}$  arises mainly from both the C=N and C=C stretching vibrations of the quinoid ring, while the band at  $\sim 1490$   $\text{cm}^{-1}$  is attributed to the C-C stretching vibration of the benzenoid ring. These bands are essential for the characterization of PANi as they provide information concerning its redox state. The band at  $\sim 1290$   $\text{cm}^{-1}$  corresponds to the C-N stretching in the secondary aromatic amine, and its high intensity indicates the presence of long conjugated length along the polymer chains.<sup>18</sup> The typical band at  $\sim 1250$   $\text{cm}^{-1}$  is related to the C-N<sup>+</sup> stretching vibration in the conducting form. The strong band at  $\sim 1140$   $\text{cm}^{-1}$  is attributed to the C-H aromatic in-plane bending vibration, which could be described as an “electronic-like band,” demonstrating a fully doped conducting PANi. The intensity ratio of quinoid (Q) to benzenoid (B) structures ( $I_Q/I_B$ ) can be used to estimate the oxidation state of PANi.<sup>18,19</sup> The ( $I_Q/I_B$ ) ratio for

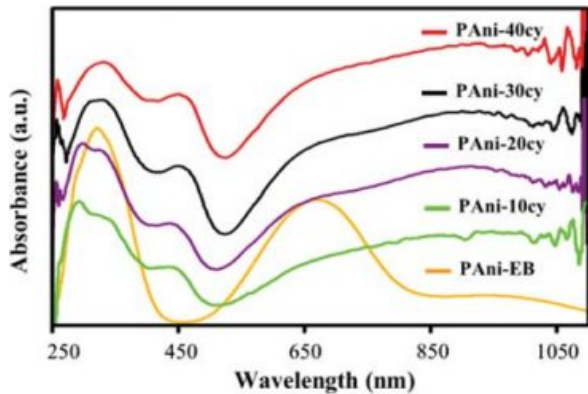


**Figure 4.** UV-Vis spectra of PANi-EB and PANi obtained for different cycle numbers (10, 20, 30, and 40).

PANi-10cy was 0.89, indicating that there are more benzenoid units within the polymer. The ( $I_Q/I_B$ ) ratio value of  $\sim 1.0$  for PANi-20cy, PANi-30cy, and PANi-40cy indicates a conducting form for the emeraldine oxidation state of PANi.

UV-Vis spectroscopy provides information on the electronic transitions between energy bands formed by  $\pi$ -conjugation along the polymer backbone. Figure 4 shows the UV-Vis absorption spectra of PANi-EB and conducting PANi obtained at different cycle numbers (10, 20, 30, and 40), which are dissolved in DMSO. HCl-doped PANi was de-doped using sodium hydroxide to obtain PANi-EB. The UV-Vis spectrum of de-doped PANi-EB shows two characteristic absorption bands at  $\sim 330$  and  $\sim 650$  nm, which can be assigned to the  $\pi$ - $\pi^*$  transition of the benzenoid rings and the excitation absorption of the quinoid rings, respectively. The doping process of conducting polymers introduce charge carriers (polaron and bipolaron) into the polymer and renders it conductive, leading to a change in its UV-Vis absorption spectrum.<sup>10</sup> Upon doping, the quinoid transition at  $\sim 650$  nm disappears, and two new absorption bands appear. These new absorption bands are attributed to the bipolaron and polaron transitions at  $\sim 450$  and  $\sim 780$  nm, respectively.<sup>20</sup> The decrease in absorbance at  $\sim 650$  nm indicates that the imine nitrogen atoms of the quinoid rings are converted to benzenoid rings by protonation with the HCl dopant, which can be attributed to the steric effect of dopant anions. As the number of cycles increases from 10 to 40, a red-shift of the  $\pi$ - $\pi^*$  transition is observed for the 304 nm and 336 nm bands, demonstrating a smaller energy gap.<sup>19</sup> Previous research showed that, with increase of the doping level, the absorption at  $\sim 650$  nm decreases while that of the  $\sim 780$  nm increases.<sup>7,10</sup> A broad absorbance at wavelengths greater than  $\sim 800$  nm is related to the presence of free carrier tails, which

is associated with an increased delocalized polaron band. As the conjugation length gets longer, the band shifts to broader wavelengths and becomes extremely large.<sup>20</sup> The doping level can be roughly estimated from the absorption spectra using the relative intensity ratio of absorbance at  $\sim 780$  nm ( $\pi$ -polaron transition) and  $\sim 330$  nm ( $\pi$ - $\pi^*$  transition).<sup>21</sup> The measured relative intensity ratios ( $I_{\sim 780}/I_{\sim 330}$ ) were 0.72, 0.88, 0.97, and 0.99 for the 10, 20, 30, and 40 cycles, respectively. The highest ( $I_{\sim 780}/I_{\sim 330}$ ) ratio observed for PANi-40cy indicates that as the number of cycles increases, it becomes easier for the counter ions to diffuse into the film, yielding higher doping levels.

The electrodeposition of PANi involves both nucleation and growth processes, beginning with the formation of PANi nuclei on the surface of the electrode and followed by their subsequent growth.<sup>14,22</sup> Instantaneous nucleation and progressive nucleation are two types of nucleation processes. In instantaneous nucleation, nearly all nuclei are formed simultaneously, while in progressive nucleation, nuclei are continually generated throughout the polymerization process.<sup>14,23</sup> There are three types of growth processes: one-dimensional (1-D), two-dimensional (2-D) and three-dimensional (3-D). The 1-D growth process refers to growth in only one direction, perpendicular to the electrode surface. In 2-D growth, the nuclei preferably grow parallel to the electrode, and 3-D growth implies similar growth rates in both perpendicular and parallel directions.<sup>14,24</sup> The morphological variation of PANi during its growth process is shown in Figures 5 and 6. SEM images were acquired at magnifications of (a) 10 kx and (b) 50 kx. Figure 5 shows SEM images of ITO and PANi obtained at different cycles (1, 3, and 5). The significant differences between the images of ITO and PANi-1cy indicate that deposition begins in the first cycle. Initially, aniline radical cations (“oxidized species”) generated at the beginning of monomer oxidation are adsorbed onto the surface of the ITO in the first cycle, and the particles start to cover the ITO surface. No significant morphological changes were observed in the third cycle as compared to the first one, though the ITO surface was more compactly coated with the particles in the third cycle. The smooth and compact PANi film formed on the ITO surface indicates a predominance of progressive nucleation with a 2-D growth process.<sup>25</sup> In the fifth cycle, further nucleation occurs and a second layer begins to form on the first 2-D layer. Given that the doping of conducting polymers occurs after polymer formation, and that the process of film growth is faster than the doping process, it is difficult for the dopant counter ions to penetrate the film due to the lack of free volume, resulting in

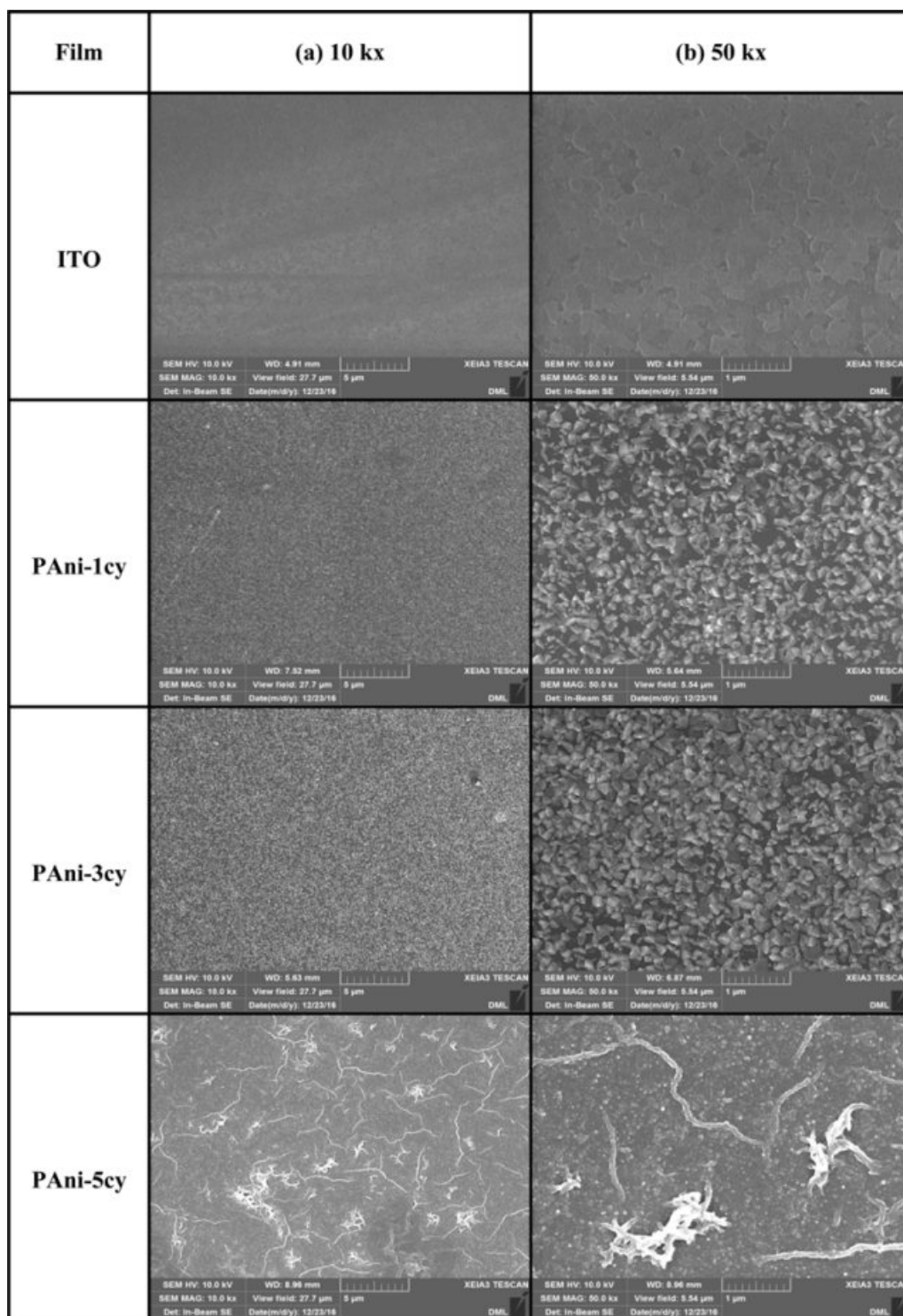


**Figure 5.** SEM images of ITO and PAni obtained for different cycle numbers (1, 3, and 5).

a low doping level for PAni.<sup>21</sup> Figure 6 shows SEM images of PAni obtained at different cycles (10, 20, 30, and 40). As the number of cycles increases, the film becomes thicker due to sequential layer-by-layer deposition. The newly formed layer

on top of the first compact layer shows an interconnected fibrous 3-D network structure after ten cycles. This fibrous morphology is inconsistent with Heinze's finding that cyclic voltammetry favors the formation of disordered chains and

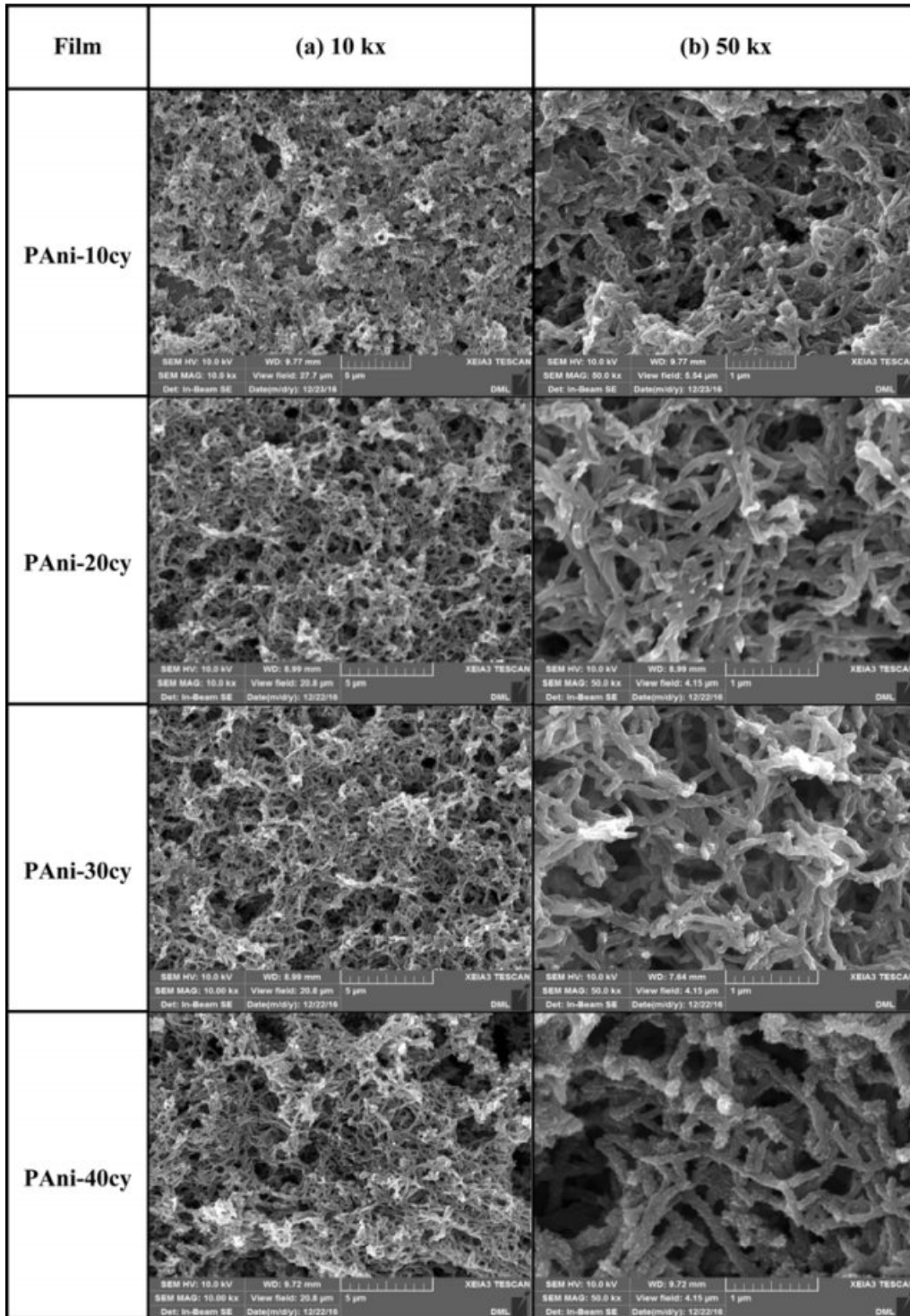


**Figure 6.** SEM images of PAni obtained for different cycle numbers (10, 20, 30, and 40).

open structures.<sup>1</sup> According to our previous studies, the fibrous porous structure is likely related to the effects of the ingress and expulsion of counter ions during each redox cycle, promoting the rearrangement of the polymeric structure.<sup>8</sup> After the

initial stage, the deposition of PAni was gradually governed by progressive nucleation with a 3-D growth process. As the number of cycles increases, the fiber thickness increases and the film adopts a rougher and more porous 3-D network struc-

**Table 1. Sheet Resistance of ITO, PAni-EB, and PAni Films Obtained for Different Cycle Numbers (10, 20, 30, and 40)**

Film	Sheet resistance (ohm/sq.)
ITO	9.55
PAni-EB	$2.00 \times 10^5$
PAni-10cy	17.51
PAni-20cy	15.53
PAni-30cy	14.75
PAni-40cy	13.86

ture. As a result, the diffusion of counter ions into the film becomes easier and the doping level is enhanced by the formation of the porous crosslinked 3-D interpenetrating polymer network.<sup>21,26</sup> In conclusion, the deposition of PAni initially occurs via progressive nucleation with a 2-D growth process, followed by progressive nucleation with a 3-D growth contribution. Thus, the number of CV cycles plays an important role in determining the morphology of the polymer and may affect the electrochemical properties of PAni.

Two-point probe methods are typically used for sheet resistance measurements. However, when the measured resistance is relatively low, four-point probe (e.g., van der Pauw) measurements are utilized as this allows for the elimination of the influence of contact resistance at the current-carrying electrodes. When the number of cycles increases, the lower part of the film deposited on the ITO surface becomes thicker than the upper part of the film as the influence of gravity becomes increasingly important. Therefore, four-point probe measurements were performed at five different locations, and the average of the measured values was used. For cycles 1, 3, and 5, the sheet resistance was not measured as the films were too thin to allow for reliable values. Table 1 shows the sheet resistances of ITO, PAni-EB, and PAni films obtained for different cycles (10, 20, 30, and 40). As the number of cycles increased, sheet resistance gradually decreased and electrical conductivity increased. As mentioned above, doping of the conducting polymers introduce charge carriers into the polymer chains that are balanced by counter ions. Since the charge carriers generated by the doping process are delocalized and provide the primary source of conduction in protonic acid doped conducting polymers, the conduction mechanism is complicated.<sup>27</sup> As expected, increasing doping levels yield an increase in electrical conduction and reduce the sheet resistance due to the formation of a porous crosslinked 3-D network between the

polymer chains and the dopant counter ions. In general, charge carrier mobility along a polymer chain (intra-chain) is higher than the mobility of charge carriers hopping between adjacent chains (inter-chain). Therefore, the thicker chain alignment in the PAni-40cy enhances charge carrier transport along the polymer chains, affecting its macroscopic electrical conduction. In conclusion, the conduction mechanism is affected by the doping level and the conformational changes in the polymer chains and relies on both the intra-chain movement of charge carriers along polymer chains and the inter-chain charge transport between adjacent chains.<sup>28,29</sup>

## Conclusions

Understanding nucleation and growth processes can provide critical insight into the formation mechanisms of PAni films on the electrode surface, allowing for the development of polymerization strategies for PAni deposition with desired electrochemical properties. In this work, the nucleation and growth processes associated with the morphological evolution of PAni during potentiodynamic polymerization were investigated. Cyclic voltammograms were recorded during the potentiodynamic growth of PAni films. Initially, progressive nucleation with a 2-D growth process predominated, followed by progressive nucleation with a 3-D growth process. The chemical structure, doping level, and morphology of PAni were found to be determined by the electrochemical properties of the films. The electrical conductance of PAni films could be controlled by modifying the polymer morphology.

## References

1. J. Heinze, B. A. Frontana-Urbe, and S. Ludwigs, *Chem. Rev.*, **110**, 4724 (2010).
2. A. Kellenberger, D. Ambros, and N. Plesu, *Int. J. Electrochem. Sci.*, **9**, 6821 (2014).
3. N. H. Khadry, M. E. Abdesalam, and G. El Enany, *J. Electrochem. Soc.*, **161**, 63 (2014).
4. H. J. N. P. D. Mello and M. Mulato, *Synth. Met.*, **239**, 66 (2018).
5. Y. Jafari, S. M. Ghoreishi, and M. Shabani-Nooshabadi, *Synth. Met.*, **217**, 220 (2016).
6. T. H. Le, Y. Kim, and H. Yoon, *Polymers(Basel)*, **9**, 150 (2017).
7. E. Kim and J.-H. Kim, *Bull. Korean Chem. Soc.*, **38**, 850 (2017).
8. E. Kim, N. Kang, J. J. Moon, and M. Choi, *Bull. Korean Chem. Soc.*, **37**, 1445 (2016).
9. E. Kim and M. Choi, *Polym. Korea*, **40**, 728 (2016).
10. E. Kim and J. Lee, *Polym. Korea*, **42**, 834 (2018).
11. M. Romero, M. A. Del Valle, R. del Río, F. R. Díaz, and F.

- Armijo, *Int. J. Electrochem. Sci.*, **7**, 10132 (2012).
12. E. Lee and E. Kim, *Bull. Korean Chem. Soc.*, **34**, 1 (2013).
  13. E. Kim, *J. Korean Chem. Soc.*, **59**, 423 (2015).
  14. M. Romero, M. A. Del Valle, R. del Río, F. R. Díaz, F. Armijo, and E. A. Dalchiele, *J. Electrochem. Soc.*, **160**, 125 (2013).
  15. D. Sazou, M. Kourouzidou, and E. Pavlidou, *Electrochim. Acta*, **52**, 4385 (2007).
  16. L. Shen and X. Huang, *Synth. Met.*, **245**, 18 (2018).
  17. G. Das and H. H. Yoon, *Int. J. Nanomedicine*, **10**, 55 (2015).
  18. F. F. Fang, Y. Z. Dong, and H. J. Choi, *Polymer(Guildf)*, **158**, 176 (2018).
  19. J. Zhao, Z. Qin, T. Li, Z. Li, Z. Zhou, and M. Zhu, *Prog. Nat. Sci. Mater. Int.*, **25**, 316 (2015).
  20. N. Karaođlan and C. Bindal, *Eng. Sci. Technol. Int. J.*, **21**, 1152 (2018).
  21. C. Liu, J. Zhang, G. Shi, and F. Chen, *J. Appl. Polym. Sci.*, **92**, 171 (2004).
  22. S. Mu and Y. Yang, *J. Phys. Chem. B*, **112**, 11558 (2008).
  23. W. Huang, J. Li, and Y. Xu, *Materials(Basel)*, **10**, 1205 (2017).
  24. M. M. Gvozdenović, B. Z. Jugović, J. S. Stevanović, and B. N. Grgur, *Hem. Ind.*, **68**, 673 (2014).
  25. Q. Qin, F. He, and W. Zhang, *J. Nanomater.*, **2016**, 1 (2016).
  26. M. Massi, C. Albonetti, M. Facchini, M. Cavallini, and F. Biscarini, *Adv. Mater.*, **18**, 2739 (2006).
  27. E. Song and J.-W. Choi, *Nanomaterials*, **3**, 498 (2013).
  28. N. Bohli, F. Gmati, A. B. Mohamed, V. Vigneras, and J. L. Miane, *J. Phys. D. Appl. Phys.*, **42**, 205404 (2009).
  29. J. A. L. Sánchez, A. M. Díez-Pascual, R. P. Capilla, and P. G. Díaz, *Polymers(Basel)*, **11**, 1032 (2019).